Pt Single Atoms Embedded in the Surface of Ni Nanocrystals as Highly Active Catalysts for Selective Hydrogenation of Nitro Compounds

Yuhan Peng,[†] Zhigang Geng,[†] Songtao Zhao,[†] Liangbing Wang,[†] Hongliang Li,[†] Xu Wang,[†,‡] Xusheng Zheng,[†] Junfa Zhu,[†] Zhenyu Li,*[,†] Rui Si,*[,‡] and Jie Zeng*[,†]

[†]Hefei National Laboratory for Physical Sciences at the Microscale, Key Laboratory of Strongly-Coupled Quantum Matter Physics of Chinese Academy of Sciences, National Synchrotron Radiation Laboratory, Department of Chemical Physics, University of Science and Technology of China, Hefei, Anhui 230026, P. R. China

[‡]Shanghai Synchrotron Radiation Facility, Shanghai Institute of Applied Physics, Chinese Academy of Sciences, Shanghai 201204, P. R. China

S Supporting Information

ABSTRACT: Single-atom catalysts exhibit high selectivity in hydrogenation due to their isolated active sites, which ensure uniform adsorption configurations of substrate molecules. Compared with the achievement in catalytic selectivity, there is still a long way to go in exploiting the catalytic activity of single-atom catalysts. Herein, we developed highly active and selective catalysts in selective hydrogenation by embedding Pt single atoms in the surface of Ni nanocrystals (denoted as Pt_1/Ni nanocrystals). During the hydrogenation of 3-nitrostyrene, the TOF numbers based on surface Pt atoms of Pt_1/Ni nanocrystals reached ~1800 h^{-1} under 3 atm of H_2 at 40 °C, much higher than that of Pt single atoms supported on active carbon, TiO_2, SiO_2, and ZSM-5. Mechanistic studies reveal that the remarkable activity of Pt_1/Ni nanocrystals derived from sufficient hydrogen supply because of spontaneous dissociation of H_2 on both Pt and Ni atoms as well as facile diffusion of H atoms on Pt_1/Ni nanocrystals. Moreover, the ensemble composed of the Pt single atom and nearby Ni atoms in Pt_1/Ni nanocrystals leads to the adsorption configuration of 3-nitrostyrene favorable for the activation of nitro groups, accounting for the high selectivity for 3-vinylaniline.

KEYWORDS: *Platinum, nickel, single atoms, selective hydrogenation, hydrogen diffusion*
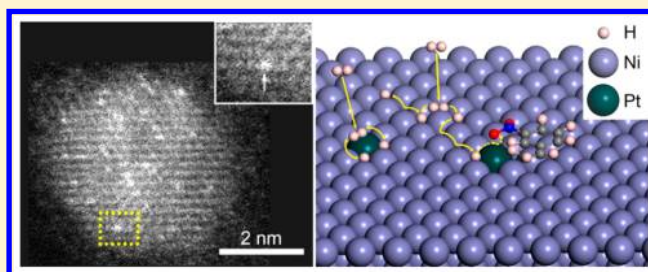
I n the past decades, great attention has been focused on selective hydrogenation reactions due to their wide applications in chemical industry.[1−8] During hydrogenation reactions, when a substrate molecule adsorbed on catalysts contains more than one unsaturated groups, the adsorption configuration is found to control the preferential activation of unsaturated groups, therefore determining the selectivity directly.[9−18] Recently, the state-of-the-art single-atom catalysts, with maximized atomic utilization efficiency up to 100%, were reported to exhibit high selectivity in hydrogenation.[19−22] The isolated active sites in single-atom catalysts ensure uniform adsorption configurations of substrate molecules, benefiting the enhancement of selectivity. For example, Pt single atoms supported on FeO_x hydrogenated 3-nitrostyrene to 3-aminostyrene showed selectivity of almost 99% due to the preferential adsorption of nitro groups.[23] Another notable example involves Pd or Pt single atoms embedded in Cu nanocrystals for selective hydrogenation of styrene, acetylene, and 1,3-butadiene, where the selectivity for the desired products was higher than 80%.[24−27] Although remarkable achievements have

been made in catalytic selectivity, there is still a long way to go in exploiting the catalytic activity of single-atom catalysts.

In the single-atom catalysts for selective hydrogenation, metal oxides, graphene, and zeolites have been applied as supports to anchor isolated active metal atoms. Unfortunately, these supports did not participate in the catalytic process because of their high energy barriers for the dissociation of H_2. In other words, active single atoms took the major responsibility for hydrogenation processes involving both the dissociation of H_2 and the addition of H atoms to substrate molecules. In general, the adsorption energy of substrate molecules is much higher than that of H_2 or H atoms on the surface of catalysts.[21,22,28,29] Accordingly, substrate molecules are more competitive than H_2 or H atoms to occupy the active sites. However, only when the dissociated H atoms diffuse to active sites could the hydrogenation be initiated, so the concentration of H atoms available to active sites affects the
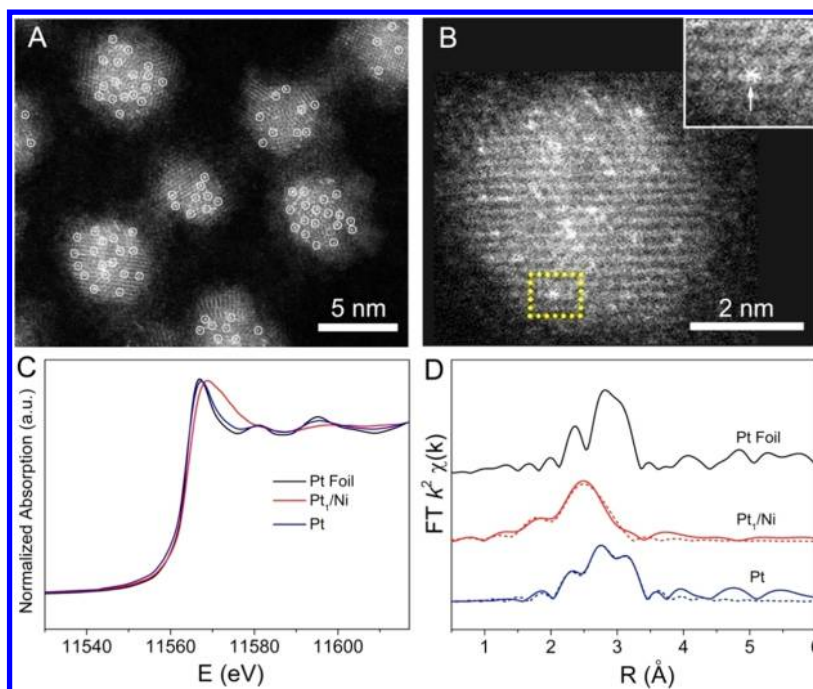
Figure 1. (A) HAADF-STEM image of 1.0%Pt$_1$/Ni nanocrystals. Pt single atoms marked in white circles were uniformly embedded in the surface of Ni nanocrystals. (B) HAADF-STEM image of an individual 1.0%Pt$_1$/Ni nanocrystal. The inset image derives from the yellow box in panel B. A Pt single atom was marked by the white arrow. (C) Pt L$_3$-edge XANES profiles of Pt foil, Pt$_1$/Ni, and Pt/C. (D) Pt L$_3$-edge EXAFS spectra in R space of Pt foil, Pt$_1$/Ni, and Pt/C. Pt foil was used as the reference.

reaction kinetics of selective hydrogenation. If H$_2$ could dissociate on the supports spontaneously and diffuse to active single atoms with ease, hydrogen supply would be sufficient for the addition of H atoms to substrate molecules. Therefore, dispersing active single atoms on supports with low energy barriers for both the dissociation of H$_2$ and the diffusion of H atoms serves as a promising strategy to improve both the activity and selectivity in selective hydrogenation but remains as a grand challenge.

Herein, we implemented this strategy by incorporating Pt single atoms in the surface of Ni nanocrystals (Pt$_1$/Ni nanocrystals). During the hydrogenation of 3-nitrostyrene, the turnover frequency (TOF) numbers based on surface Pt atoms of Pt$_1$/Ni nanocrystals were ca. 1800 h^{-1} under 3 atm of H$_2$ at 40 °C, much higher than that of Pt single atoms supported on active carbon, TiO$_2$, SiO$_2$, and ZSM-5. Besides, only nitro groups were hydrogenated over Pt$_1$/Ni nanocrystals. Mechanistic studies reveal that both Pt and Ni atoms in Pt$_1$/Ni nanocrystals allowed for the dissociation of H$_2$ and adsorption of H atoms so that an abundant amount of H atoms was produced on the surface of Pt$_1$/Ni nanocrystals. Not only were the H atoms adsorbed on Pt atoms added to 3-nitrostyrene, but the H atoms adsorbed on Ni atoms were also involved in the reaction through facilely diffusing to active Pt atoms for the subsequent hydrogenation. Moreover, the ensemble composed of the Pt single atom and nearby Ni atoms in Pt$_1$/Ni nanocrystals leads to the adsorption configuration of 3-nitrostyrene, favorable for the activation of nitro groups, accounting for the high selectivity for 3-vinylaniline.

To begin with, we prepared Ni nanocrystals with an average size of 4.4 nm (Figure S1). Pt single atoms incorporated in the surface of Ni nanocrystals were synthesized via the galvanic replacement reaction between Ni nanocrystals and Pt(acac)$_2$. In a typical synthesis, Ni nanocrystals were dispersed in hexane

under magnetic stirring, followed by the addition of Pt(acac)$_2$ solution (dissolved in toluene) through a syringe pump at the speed of 2 mL/h. Figure 1A shows a high-angle annular dark-field scanning transmission electron microscopy (HAADF-STEM) image of the obtained nanocrystals in high purity. As manifested by brightness and marked by white circles, isolated Pt atoms were uniformly embedded in the surface of Ni nanocrystals. A typical HAADF-STEM image of an individual nanocrystal was shown to highlight the dopant atoms (Figure 1B). The magnified image further confirmed the replacement of surface Ni atoms by isolated Pt atoms, where Pt single atoms were clearly marked by white arrows. As revealed by inductively coupled plasma-atomic emission spectroscopy (ICP-AES) analysis, the atomic percentage of Pt in this sample was determined as 1.0%. Thus, these nanocrystals were denoted as 1.0%Pt$_1$/Ni nanocrystals. By simply varying the amounts of added Pt(acac)$_2$ solution in synthetic process, Pt single atoms embedded in Ni nanocrystals with the Pt atomic percentages of 0.2%, 0.5%, and 1.5% were facilely prepared, donated as 0.2% Pt$_1$/Ni, 0.5%Pt$_1$/Ni, and 1.5%Pt$_1$/Ni nanocrystals, respectively. When the Pt atomic percentage was increased to 3.0%, Pt clusters with a size of ∼1.2 nm were synthesized, denoted as Pt clusters/Ni nanocrystals (Figure S2). In addition, commercial Pt/C (5 wt % on active carbon) with Pt nanocrystals taking an average size of ca. 3 nm was purchased (Figure S1). The characteristic X-ray diffraction (XRD) profile of Ni nanocrystals shows the peaks assigned to (111), (200), and (220) reflections of face-centered cubic (*fcc*) Ni (Figure S3). The peaks of Pt$_1$/Ni nanocrystals with different Pt contents were located at similar positions to those of Ni nanocrystals, whereas those of Pt/C shifted to lower angles. The ratios of surface metal atoms to total atoms in 0.2%Pt$_1$/Ni, 0.5%Pt$_1$/Ni, 1.0%Pt$_1$/Ni, and 1.5%Pt$_1$/Ni nanocrystals were determined as 31.3%, 29.7%, 30.2%, and 31.4%, respectively, by CO pulse chemisorptions,
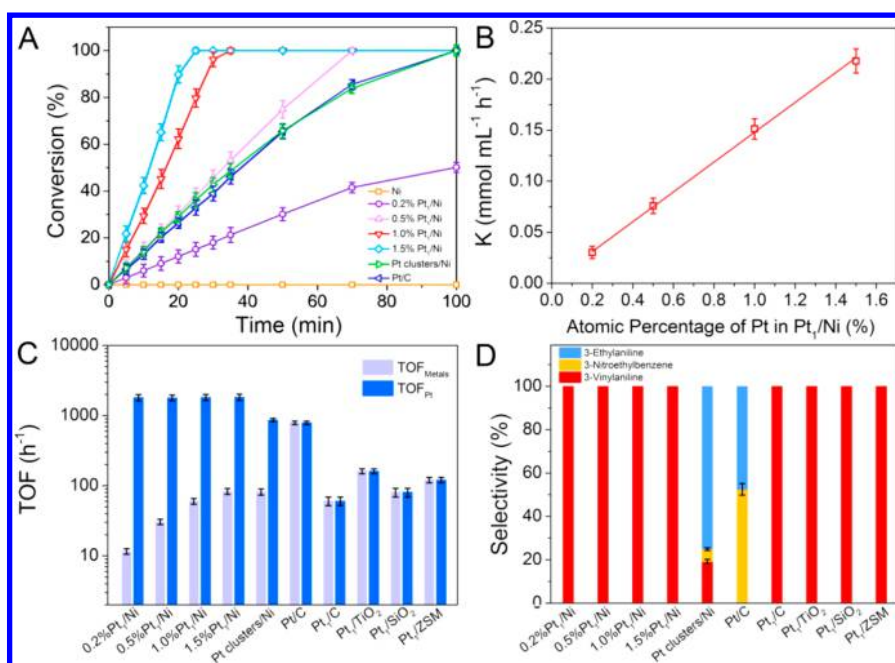
Figure 2. (A) Time courses of the conversion for Ni nanocrystals, Pt$_1$/Ni nanocrystals, Pt clusters/Ni nanocrystals, and Pt/C in selective hydrogenation of 3-nitrostyrene under 3 atm of H$_2$ at 40 °C. (B) Comparison of reaction rates for Pt$_1$/Ni nanocrystals with different Pt atomic percentages. (C) Comparison of TOF numbers for different Pt single-atom catalysts, Pt clusters/Ni nanocrystals, and Pt/C under 3 atm of H$_2$ at 40 °C. (D) Comparison of selectivity for Pt single-atom catalysts, Pt clusters/Ni nanocrystals, and Pt/C under 3 atm of H$_2$ at 40 °C after 100 min. Error bars represent standard deviation from three independent measurements.

while those in Pt clusters/Ni nanocrystals and Pt/C were 31.8% and 36.4%, respectively (Figure S4).

The X-ray absorption near-edge spectroscopy (XANES) and extended X-ray absorption fine structure (EXAFS) spectra were measured to determine the electronic and coordination structures. As shown in Figure 1C, the white lines (the biggest jump in edge) of the samples were located around 11570 eV, reflecting the oxidation states of Pt species.[30] The similarity in intensity of white lines among Pt$_1$/Ni nanocrystals, Pt/C, and Pt foil indicates that Pt species in Pt$_1$/Ni nanocrystals were dominant in metallic state. Pt single atoms in the surface of Ni nanocrystals were identified by the EXAFS spectra of Pt$_1$/Ni nanocrystals (Figure 1D). For 0.2%Pt$_1$/Ni, 0.5%Pt$_1$/Ni, 1.0% Pt$_1$/Ni, and 1.5%Pt$_1$/Ni nanocrystals, only Pt–Ni shell at 2.57−2.59 Å with a coordination number (CNs) of 5.6–6.1 was observed without any contribution from Pt–Pt shell (Table S1). The spectrum of Pt/C only showed a Pt–Pt shell at 2.76 Å with a CN of 7.3. Based on the CN of Pt–Pt shell, the average grain size was estimated as ca. 3 nm.[31]

The catalytic properties of Pt$_1$/Ni nanocrystals were explored toward hydrogenation of 3-nitrostyrene in comparison with Pt clusters/Ni nanocrystals, Ni nanocrystals, and Pt/C. Before catalytic tests, the as-synthesized nanocrystals were cleaned by plasma treatment with a power of 40 W under 5 Pa of H$_2$ for 40 min.[32,33] The peaks for oleylamine disappeared after plasma treatment, indicating the removal of the organic capping molecules (Figure S5). As shown in Figure 2A, Ni nanocrystals were inert, whereas Pt-based catalysts exhibited catalytic activity. Moreover, the reaction rates for different Pt$_1$/Ni nanocrystals were in direct proportion to the atomic percentage of Pt (Figure 2B). As a result, Pt single atoms served as active sites in Pt$_1$/Ni nanocrystals for selective hydrogenation of 3-nitrostyrene at 40 °C.

We further calculated the TOF numbers based on all surface metal atoms (denoted as TOF$_{Metals}$) of Pt$_1$/Ni nanocrystals and Pt/C. The TOF$_{Metals}$ numbers of 0.2%Pt$_1$/Ni, 0.5%Pt$_1$/Ni, 1.0% Pt$_1$/Ni, and 1.5%Pt$_1$/Ni nanocrystals were 12, 31, 60, and 83 h^{-1}, whereas those of Pt clusters/Ni nanocrystals and Pt/C were 82 and 789 h^{-1}, respectively (Figure 2C, Table S2). The TOF numbers of Pt$_1$/Ni nanocrystals based on Pt atoms (TOF$_{Pt}$) were ca. 1800 h^{-1}, regardless of different Pt contents, higher than that (865 h^{-1}) of Pt clusters/Ni nanocrystals (Figure 2C). To investigate the role of supports, we also deposited Pt single atoms on active carbon, TiO$_2$, SiO$_2$, and ZSM-5, denoted as Pt$_1$/C, Pt$_1$/TiO$_2$, Pt$_1$/SiO$_2$, and Pt$_1$/ZSM, respectively (Figure S6). The TOF$_{Pt}$ numbers of Pt$_1$/C, Pt$_1$/TiO$_2$, Pt$_1$/SiO$_2$, and Pt$_1$/ZSM were 60, 161, 80, and 121 h^{-1}, respectively, much lower than those of Pt$_1$/Ni nanocrystals (Figure 2C, Table S2). As such, Ni nanocrystals played a pivotal role in enhancing the catalytic activity of Pt$_1$/Ni nanocrystals.

We further explored the catalytic selectivity in hydrogenation of 3-nitrostyrene. As for Pt single-atom catalysts, only nitro groups were hydrogenated, with the selectivity of >99% for 3-vinylaniline (Figures 2D, S7, and S8). For Pt clusters/Ni nanocrystals and Pt/C, both nitro groups and carbon–carbon double bonds were simultaneously hydrogenated. After 100 min, the selectivity for 3-vinylaniline, 3-nitroethylbenzene, and 3-ethylaniline was 19%, 6%, and 75%, respectively, for Pt clusters/Ni nanocrystals. As for Pt/C, 48% of 3-ethylaniline and 52% of 3-nitroethylbenzene were formed after 100 min (Figure 2D). We further applied 1.0%Pt$_1$/Ni nanocrystals in the selective hydrogenation of 15 nitro compounds to explore the applicability. Besides nitro groups, these substrate molecules contained other sensitive functional groups, including esters, ketone, aldehyde, halogen, and cyano. The conversion of these substrate molecules reached >97% over 1.0%Pt$_1$/Ni nanocryst-
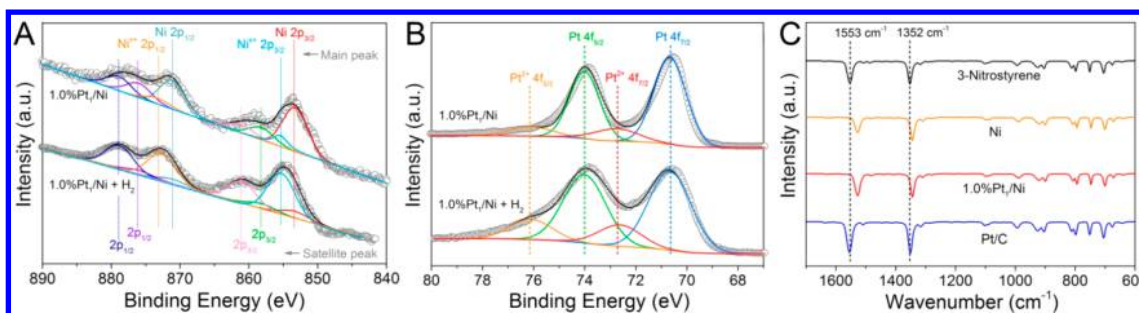
Figure 3. *In situ* XPS spectra of (A) Ni 2p and (B) Pt 4f for 1.0%Pt$_1$/Ni nanocrystals before/after the treatment of the samples with H$_2$ at 40 °C for 30 min, respectively. (C) IR spectrum of 3-nitrostyrene and *in situ* DRIFTS spectra of Ni nanocrystals, 1.0%Pt$_1$/Ni nanocrystals, and Pt/C. *In situ* DRIFTS spectra were obtained after the exposure of nanocrystals to 3-nitrostyrene at 40 °C for 30 min.
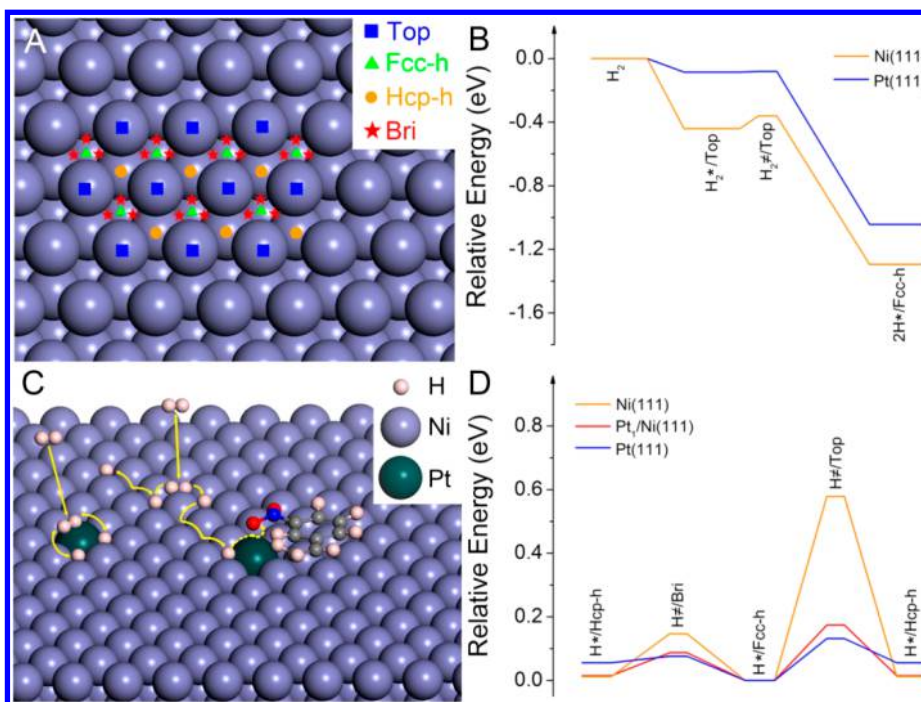

Figure 4. (A) Top view of typical adsorption sites of H atoms on (111) facet of metal surface. Site Top, Fcc-h, Hcp-h, and Bri represent top, *fcc*-hollow, *hcp*-hollow, and bridge sites, respectively. (B) Potential energy profiles of the dissociation of H$_2$ on Ni(111) and Pt(111). The energy barrier of H$_2$ dissociation on Ni(111) is 0.08 eV. (C) Schematic illustration of H$_2$ dissociation and H diffusion on Pt$_1$/Ni(111). (D) Diffusion paths of H atoms on Ni(111), Pt$_1$/Ni(111), and Pt(111). The symbols * and ≠ in panels B and D represent the adsorbed and transitional states, respectively.

als under 3 atm of H$_2$ at 40 °C after 100 min (Figure S9). Moreover, only nitro groups were hydrogenated in all the substrate molecules, with the selectivity of >95% for amino compounds. In addition, we further investigate the stability of 1.0%Pt$_1$/Ni nanocrystals. After ten successive reaction rounds, 97% of activity and 98% of selectivity for nitro groups were preserved (Figure S10). Moreover, the HAADF-STEM image of 1.0%Pt$_1$/Ni nanocrystals after ten rounds shows the absence of Pt clusters, indicating that Pt atoms were still atomically dispersed on Ni nanocrystals. Thus, Pt$_1$/Ni nanocrystals exhibited high stability during the selective hydrogenation.

The adsorption properties of H$_2$ on the surface of 1.0%Pt$_1$/Ni nanocrystals were investigated through *in situ* X-ray photoelectron spectroscopy (XPS) measurements. The 1.0% Pt$_1$/Ni nanocrystals were exposed to H$_2$ at 40 °C for 30 min in a reaction cell attached to the XPS end-station, followed by measurements of *in situ* XPS. The XPS spectra of Ni 2p and Pt 4f indicated that the majority of surface Ni and Pt species was in the metallic states (Figure 3A,B). After the sample had been

exposed to H$_2$, the ratios of both Pt^{2+} and Ni^{x+} on the surface increased, as a result of the electron transfer from surface metal atoms to adsorbed H atoms.[34] The XPS results indicated the presence of H atoms on both surface Pt and Ni atoms. This point was further identified by *in situ* diffuse reflectance infrared Fourier transform spectroscopy (DRIFTS) after the treatment with H$_2$ at 40 °C for 30 min. The peaks at 1948 and 1596 cm^{-1} for Pt/C and Ni nanocrystals corresponded to the stretching vibrations of Pt−H and Ni−H, respectively (Figure S11). For 1.0%Pt$_1$/Ni nanocrystals, both stretching vibrations of Ni−H and Pt−H were clearly observed. In addition, the peak for Pt−H in 1.0%Pt$_1$/Ni nanocrystals blue-shifted to 1985 cm^{-1}, due to the unique coordination environment of Pt single atoms (Figure S11).

The interaction between 3-nitrostyrene and catalysts was explored via *in situ* DRIFTS analysis. Figure 3C reveals *in situ* DRIFTS spectra of Ni, Pt, and 1.0%Pt$_1$/Ni nanocrystals after the treatment with 3-nitrostyrene at 40 °C. In the absence of catalysts, the spectrum of 3-nitrostyrene exhibited two peaks at

1553 and 1352 cm^{-1} for the asymmetrical and symmetrical stretching vibrations of nitro groups, respectively. With regard to Ni nanocrystals after the exposure to 3-nitrostyrene, the peaks assigned to the asymmetrical and symmetrical stretching vibrations of nitro groups respectively red-shifted by 25 and 6 cm^{-1} compared with those for free 3-nitrostyrene. The red shifts indicate the weakening of N=O bonds and thus a strong interaction between nitro groups and surface Ni atoms. As for Pt/C, the variation in the peaks for nitro groups was negligible, relative to those for free 3-nitrostyrene, indicating a weak interaction between nitro groups and Pt atoms. In comparison, the peaks for 1.0%Pt$_1$/Ni nanocrystals were located at positions similar to those for Ni nanocrystals. As such, the nitro groups strongly interacted with 1.0%Pt$_1$/Ni and Ni nanocrystals.

To investigate how the adsorption of 3-nitrostyrene on Ni nanocrystals influenced the dissociation of H$_2$, we conducted *in situ* DRIFTS measurements of Ni and Pt$_1$/Ni nanocrystals after the treatment with 3-nitrostyrene and H$_2$ in sequence. For Ni nanocrystals, besides the peak for adsorbed nitro groups, the peak for Ni−H appeared (Figure S11). As such, the surfaces of Ni nanocrystals were not fully blocked by 3-nitrostyrene due to the steric effect and still able to dissociate H$_2$. For Pt$_1$/Ni nanocrystals, the peaks for Ni−H and Pt−H were still observed. Moreover, the peak for nitro groups disappeared, while a new peak at 3301 cm^{-1} assigned to the stretching vibration of −NH$_2$ was formed. In this case, nitro groups were hydrogenated into −NH$_2$ on Pt$_1$/Ni nanocrystals. Furthermore, we conducted solid-state deuterium-nuclear magnetic resonance (D-NMR) experiments. After the adsorption of 3-nitrostyrene, the peak intensity in the solid-state D-NMR spectrum of Ni nanocrystals was weaker than that without the adsorption of substrate molecules. Therefore, the adsorption of 3-nitrostyrene blocked a proportion of surface Ni atoms, impeding the dissociation of H$_2$ on Ni nanocrystals.

To rationalize the remarkable catalytic activity and selectivity of Pt$_1$/Ni nanocrystals for the selective hydrogenation, we carried out density functional theory (DFT) calculations. Besides Ni(111) and Pt(111) models terminated by (111) facets, the model of a Pt single atom in Ni(111) was also built, denoted as Pt$_1$/Ni(111) (Figure S12). Four sites, including top, *fcc*-hollow, hexagonal close-packed (*hcp*)-hollow, and bridge sites, exist on metal surface (Figure 4A). The dissociation of H$_2$ over the top sites of surface Pt atoms has no energy barrier (Figure 4B). As for Ni(111), the low energy barrier of 0.08 eV also ensures spontaneous dissociation of H$_2$ even at 40 °C (Figure 4B).

To further explore the origin of catalytic activity, we examined the hydrogen diffusion process on different metal surfaces. H atoms generally add to substrate molecules only at top sites of active metal atoms.[35−40] In this case, H atoms diffuse from hollow sites to top sites. For Ni(111), Pt(111), and Pt$_1$/Ni(111), the adsorption of H atoms on *fcc*-hollow sites has the lowest energy among H adsorption on different sites (Figure 4D). As such, H diffusion process is regarded to initiate from *fcc*-hollow sites. In this case, the energy barrier for H atoms to diffuse from *fcc*-hollow to *hcp*-hollow sites through bridge sites is denoted as $E_{\text{a-supply}}$, while that for the diffusion of H atoms from *fcc*-hollow to top sites is named as $E_{\text{a-react}}$. The values of $E_{\text{a-supply}}$ are <0.2 eV for both Ni and Pt atoms on Ni(111), Pt(111), and Pt$_1$/Ni(111), guaranteeing the diffusion of H atoms on these surfaces with ease at 40 °C (Figure 4D). With regard to $E_{\text{a-react}}$, the values over Pt atoms on Pt(111) and Pt$_1$/Ni(111) are 0.13 and 0.17 eV, respectively (Figure 4D). In

comparison, Ni atoms on Ni(111) and Pt$_1$/Ni(111) show the values of $E_{\text{a-react}}$ above 0.5 eV (Figures 4D and S13), accounting for that Ni atoms were inert at 40 °C despite of their ability to adsorb nitro groups (Figure 3C). Therefore, $E_{\text{a-react}}$ is proposed as a descriptor of catalytic activity. Pt single atoms in Pt$_1$/Ni(111) serve as the active center due to the much lower $E_{\text{a-react}}$ relative to that for Ni atoms.

Based on DFT results, a schematic illustration is provided to show hydrogen dissociation and diffusion on Pt$_1$/Ni(111) (Figure 4C). All the surface atoms, either Pt or Ni atoms, contribute to the dissociation of H$_2$ molecules, resulting in the abundant H atoms on Pt$_1$/Ni(111). In other words, Ni nanocrystals serve as a support to anchor Pt single atoms in Pt$_1$/Ni(111) and a reservoir to provide active H atoms that facilitate the hydrogenation reactions. For Pt$_1$/Ni nanocrystals, not only were the H atoms adsorbed on Pt atoms added to 3-nitrostyrene, but the H atoms adsorbed on Ni atoms were also involved in the catalytic reaction through the diffusion process. Therefore, the high activity of Pt$_1$/Ni nanocrystals derived from sufficient hydrogen supply.

As for catalytic selectivity, we conducted DFT calculations to investigate the optimized adsorption configuration of 3-nitrostyrene on Ni(111), Pt$_1$/Ni(111), and Pt(111). With regard to Ni(111), the distances from two O atoms in the nitro group to the nearest surface Ni atoms are 2.01 and 2.02 Å, respectively (Figures S14−S15 and Table S3). Accordingly, nitro groups could be activated efficiently by accepting 0.61 electrons from surface Ni atoms. However, the large $E_{\text{a-react}}$ value on Ni(111) impedes the hydrogenation of activated nitro groups into amino groups on Ni(111) at room temperature. In contrast, O atoms are far away from surface Pt atoms with the distance >3 Å on Pt(111), accepting only 0.01 electron and thereby indicating the weak interaction between nitro groups and Pt nanocrystals (Table S3). As for Pt$_1$/Ni(111), the adsorbed 3-nitrostyrene on pure Ni atoms takes the similar configuration to that on Ni(111) and is unable to be hydrogenated due to the large $E_{\text{a-react}}$ value. In this case, only the adsorption of 3-nitrostyrene on Pt single atoms is taken into consideration. The distance from one O atom in the nitro group to a Pt single atom is 2.26 Å, while that from the other O atom to the nearest Ni atom is 2.03 Å (Table S3). The donated electrons from Pt atoms to O atoms are 0.54 electrons, comparable to those on Ni(111). Thus, the ensemble composed of the Pt single atom and nearby Ni atoms induces the adsorption configuration of 3-nitrostyrene, favorable for the activation of nitro groups, accounting for the high selectivity for 3-vinylaniline over Pt$_1$/Ni nanocrystals.

Moreover, a nitrostyrene molecule mainly contains two types of unsaturated functional groups including carbon−carbon double bonds and nitro groups. The selective hydrogenation of carbon−carbon double bonds is reported to be highly sensitive to the size of Pt ensembles.[38] Specifically, the selectivity for carbon−carbon double bonds drops with the decreased size of Pt, particular for Pt single atoms.[23,25,41] As for the nitro groups, the selectivity for them is independent of the size of Pt.[41] Noteworthy, Pt single atoms especially prefer the adsorption of nitro groups.[23] Therefore, Pt single atoms both block the hydrogenation of carbon−carbon double bonds and benefit the activation of nitro groups, accounting for the high selectivity for 3-vinylaniline over Pt$_1$/Ni nanocrystals.

In conclusion, we report a superior selective hydrogenation catalyst by embedding Pt single atoms in the surface of Ni nanocrystals. During the hydrogenation of 3-nitrostyrene, Pt$_1$/

Ni nanocrystals achieved the TOF numbers of ca. 1800 h^{-1} based on surface Pt atoms under 3 atm of H$_2$ at 40 °C. According to mechanistic studies, the remarkable activity of Pt$_1$/Ni nanocrystals derived from sufficient hydrogen supply because of spontaneous dissociation of H$_2$ on both Pt and Ni atoms as well as facile diffusion of H atoms on Ni nanocrystals. Moreover, the high selectivity for 3-vinylaniline was ascribed to that the adsorption configuration of 3-nitrostyrene on the ensemble composed of the Pt single atom and nearby Ni atoms in Pt$_1$/Ni nanocrystals favored the activation of nitro groups. The deposition of single atoms on supports with low energy barriers for hydrogen dissociation and diffusion not only offers a powerful means to improve the catalytic performance for selective hydrogenation but also extends our understanding of single-atom catalysis.

■ ASSOCIATED CONTENT

Ⓢ Supporting Information

The Supporting Information is available free of charge on the ACS Publications website at DOI: 10.1021/acs.nanolett.8b01059.

> Experimental details, TEM image, HAADF-STEM image of Pt clusters/Ni nanocrystals, size distribution diagram, XRD patterns, CO pulse chemisorption profiles, EXAFS data fitting results, IRRAS spectra of pure OAm and 1.0% Pt$_1$/Ni nanocrystals before/after plasma treatment, comparison of TOF numbers, HAADF-STEM images, time courses of hydrogenation of 3-nitrostyrene, hydrogenation of various nitro compounds, stability tests, *in situ* DRIFTS spectra of Ni and 1.0%Pt$_1$/Ni nanocrystals after different gas treatment, DFT models, comparison of $E_{\text{a-react}}$ over Pt and Ni atoms, top views of the adsorption configuration of 3-nitrostyrene on different metal surfaces, adsorption configurations and differential charge densities of 3-nitrostyrene on different metal surfaces, adsorption energies of 3-nitrostyrene, and distance from the functional group to the nearest metal atoms on different metal surfaces (PDF)

■ AUTHOR INFORMATION

Corresponding Authors
*E-mail: zyli@ustc.edu.cn (Z.L.).
*E-mail: sirui@sinap.ac.cn (R.S.).
*E-mail: zengj@ustc.edu.cn (J.Z.).

ORCID Ⓞ
Junfa Zhu: 0000-0003-0888-4261
Zhenyu Li: 0000-0003-2112-9834
Jie Zeng: 0000-0002-8812-0298

Author Contributions
Y.P., Z.G., and S.Z. contributed equally.

Notes
The authors declare no competing financial interest.

■ ACKNOWLEDGMENTS

■ REFERENCES

(1) Wang, L.; Zhang, W.; Zheng, X.; Chen, Y.; Wu, W.; Qiu, J.; Zhao, X.; Zhao, X.; Dai, Y.; Zeng, J. *Nature Energy* **2017**, *2*, 869−876.

(2) Zhao, M.; Yuan, K.; Wang, Y.; Li, G.; Guo, J.; Gu, L.; Hu, W.; Zhao, H.; Tang, Z. *Nature* **2016**, *539*, 76−80.

(3) Cui, X.; Surkus, A.; Junge, K.; Topf, C.; Radnik, J.; Kreyenschulte, C.; Beller, M. *Nat. Commun.* **2016**, *7*, 11326.

(4) Zhang, Z.; Zhu, Y.; Asakura, H.; Zhang, B.; Zhang, J.; Zhou, M.; Han, Y.; Tanaka, T.; Wang, A.; Zhang, T.; Yan, N. *Nat. Commun.* **2017**, *8*, 16100.

(5) Cisneros, L.; Serna, P.; Corma, A. *Angew. Chem., Int. Ed.* **2014**, *53*, 9306−9310.

(6) Khan, M. U.; Wang, L.; Liu, Z.; Gao, Z.; Wang, S.; Li, H.; Zhang, W.; Wang, M.; Wang, Z.; Ma, C.; Zeng, J. *Angew. Chem., Int. Ed.* **2016**, *55*, 9548−9552.

(7) Serna, P.; Corma, A. *ACS Catal.* **2015**, *5*, 7114−7121.

(8) Kuo, C.-H.; Tang, Y.; Chou, L.-Y.; Sneed, B. T.; Brodsky, C. N.; Zhao, Z.; Tsung, C.-K. *J. Am. Chem. Soc.* **2012**, *134*, 14345−14348.

(9) Wang, L.; Zhang, W.; Wang, S.; Gao, Z.; Luo, Z.; Wang, X.; Zeng, R.; Li, A.; Li, H.; Wang, M.; Zheng, X.; Zhu, J.; Zhang, W.; Ma, C.; Si, R.; Zeng, J. *Nat. Commun.* **2016**, *7*, 14036.

(10) Adam, R.; Cabrero-Antonino, J. R.; Spannenberg, A.; Junge, K.; Jackstell, R.; Beller, M. *Angew. Chem.* **2017**, *129*, 3264−3268.

(11) Hao, C.-H.; Guo, X.-N.; Pan, Y.-T.; Chen, S.; Jiao, Z.-F.; Yang, H.; Guo, X.-Y. *J. Am. Chem. Soc.* **2016**, *138*, 9361−9364.

(12) Tan, Y.; Liu, X.; Zhang, L.; Wang, A.; Li, L.; Pan, X.; Haruta, M.; Wei, H.; Wang, H.; Wang, F.; Wang, X.; Zhang, T. *Angew. Chem., Int. Ed.* **2017**, *56*, 2709−2713.

(13) Miyazaki, M.; Furukawa, S.; Komatsu, T. *J. Am. Chem. Soc.* **2017**, *139*, 18231−18239.

(14) Li, G.; Abroshan, H.; Chen, Y.; Jin, R.; Kim, H. J. *J. Am. Chem. Soc.* **2015**, *137*, 14295−14304.

(15) Schrader, I.; Warneke, J.; Backenköhler, J.; Kunz, S. *J. Am. Chem. Soc.* **2015**, *137*, 905−912.

(16) Ye, T.-N.; Lu, Y.; Li, J.; Nakao, T.; Yang, H.; Tada, T.; Kitano, M.; Hosono, H. *J. Am. Chem. Soc.* **2017**, *139*, 17089−17097.

(17) Gawande, M. B.; Zboril, R.; Malgras, V.; Yamauchi, Y. *J. Mater. Chem. A* **2015**, *3*, 8241−8245.

(18) Marshall, S. T.; O'Brien, M.; Oetter, B.; Corpuz, A.; Richards, R. M.; Schwartz, D. K.; Medlin, J. W. *Nat. Mater.* **2010**, *9*, 853−858.

(19) Zhang, H.; Watanabe, T.; Okumura, M.; Haruta, M.; Toshima, N. *Nat. Mater.* **2012**, *11*, 49−52.

(20) Wang, X.; Chen, W.; Zhang, L.; Yao, T.; Liu, W.; Lin, Y.; Ju, H.; Dong, J.; Zheng, L.; Yan, W.; Zheng, X.; Li, Z.; Wang, X.; Yang, J.; He, D.; Wang, Y.; Deng, Z.; Wu, Y.; Li, Y. *J. Am. Chem. Soc.* **2017**, *139*, 9419−9422.

(21) Vilé, G.; Albani, D.; Nachtegaal, M.; Chen, Z.; Dontsova, D.; Antonietti, M.; Lopez, N.; Pérez-Ramírez, J. *Angew. Chem., Int. Ed.* **2015**, *54*, 11265−11269.

(22) Zhang, S.; Chang, C.-R.; Huang, Z.-Q.; Li, J.; Wu, Z.; Ma, Y.; Zhang, Z.; Wang, Y.; Qu, Y. *J. Am. Chem. Soc.* **2016**, *138*, 2629−2637.

(23) Wei, H.; Liu, X.; Wang, A.; Zhang, L.; Qiao, B.; Yang, X.; Huang, Y.; Miao, S.; Liu, J.; Zhang, T. *Nat. Commun.* **2014**, *5*, 5634.

(24) Kyriakou, G.; Boucher, M. B.; Jewell, A. D.; Lewis, E. A.; Lawton, T. J.; Baber, A. E.; Tierney, H. L.; Flytzani-Stephanopoulos, M.; Sykes, E. C. H. *Science* **2012**, *335*, 1209−1212.

(25) Lucci, F. R.; Liu, J.; Marcinkowski, M. D.; Yang, M.; Allard, L. F.; Flytzani-Stephanopoulos, M.; Sykes, E. C. H. *Nat. Commun.* **2015**, *6*, 8550.

(26) Boucher, M. B.; Zugic, B.; Cladaras, G.; Kammert, J.; Marcinkowski, M. D.; Lawton, T. J.; Sykes, E. C. H.; Flytzani-Stephanopoulos, M. *Phys. Chem. Chem. Phys.* **2013**, *15*, 12187−12196.

(27) Lang, R.; Li, T.; Matsumura, D.; Miao, S.; Ren, Y.; Cui, Y.-T.; Tan, Y.; Qiao, B.; Li, L.; Wang, A.; Wang, X.; Zhang, T. *Angew. Chem., Int. Ed.* **2016**, *55*, 16054−16058.

(28) Kruppe, C. M.; Krooswyk, J. D.; Trenary, M. *ACS Catal.* **2017**, *7*, 8042−8049.

(29) Humbert, M. P.; Chen, J. G. *J. Catal.* **2008**, *257*, 297−306.

(30) Yoshida, H.; Nonoyama, S.; Yazawa, Y.; Hattori, T. *Phys. Scr.* **2005**, *T115*, 813.

(31) Frenkel, A. I.; Hills, C. W.; Nuzzo, R. G. *J. Phys. Chem. B* **2001**, *105*, 12689−12703.

(32) Antoniak, C.; Lindner, J.; Spasova, M.; Sudfeld, D.; Acet, M.; Farle, M.; Wilhelm, F.; Rogalev, A.; Sun, S. *Phys. Rev. Lett.* **2006**, *97*, 117201.

(33) Antoniak, C.; Gruner, M. E.; Spasova, M.; Trunova, A. V.; Römer, F. M.; Warland, A.; Krumme, B.; Fauth, K.; Sun, S.; Farle, M.; Wende, H. *Nat. Commun.* **2011**, *2*, 528.

(34) Syrenova, S.; Wadell, C.; Nugroho, F. A. A.; Gschneidtner, T. A.; Fernandez, Y. A. D.; Nalin, G.; Switlik, D.; Westerlund, F.; Antosiewicz, T. J.; Zhdanov, V. P.; Moth-Poulsen, K.; Langhammer, C. *Nat. Mater.* **2015**, *14*, 1236−1244.

(35) Mahata, A.; Rai, R. K.; Choudhuri, I.; Singh, S. K.; Pathak, B. *Phys. Chem. Chem. Phys.* **2014**, *16*, 26365−26374.

(36) Zhang, L.; Jiang, J.; Shi, W.; Xia, S.; Ni, Z.; Xiao, X. *RSC Adv.* **2015**, *5*, 34319−34326.

(37) Neurock, M.; Pallassana, V.; van Santen, R. A. *J. Am. Chem. Soc.* **2000**, *122*, 1150−1153.

(38) Lyu, J.; Wang, J.; Lu, C.; Ma, L.; Zhang, Q.; He, X.; Li, X. *J. Phys. Chem. C* **2014**, *118*, 2594−2601.

(39) Andersin, J.; Lopez, N.; Honkala, K. *J. Phys. Chem. C* **2009**, *113*, 8278−8286.

(40) Yang, B.; Burch, R.; Hardacre, C.; Headdock, G.; Hu, P. *J. Catal.* **2013**, *305*, 264−276.

(41) Corma, A.; Serna, P.; Concepción, P.; Calvino, J. J. *J. Am. Chem. Soc.* **2008**, *130*, 8748−8753.